

140

**NASA TECHNICAL
MEMORANDUM**

NASA TM X- 62,260

NASA TM X- 62,260

SPIN SCAN IMAGING AT JUPITER

Kenneth F. Sinclair

**Ames Research Center
Moffett Field, Calif. 94035**

(NASA-TM-X-62260) SPIN SCAN IMAGING AT
JUPITER (NASA) 37 p HC \$4.00 CSCL 03B

N73-24836

G3/30 Unclass
 04710

April 1973

Table of Contents

	Page
Introduction	1
Data Requirements for Imaging Experiments	2
Spin Scan Camera	4
Camera Description	4
Camera Selection	5
Operational Considerations	9
Preliminary Camera Design	21
Camera Model	21
Baseline Camera	29
Concluding Remarks	29
References	34

List of Illustrations

Figure		Page
1	Typical Spacecraft and Camera Geometry near Jupiter	6
2	Multi-Detector Data Handling	7
3	Camera Resolution	8
4	Camera Performance Characteristics	11
5	Typical Jupiter Orbit	12
6	1976 Encounter Characteristics: (a) Jupiter; (b) Io	16
	(c) Europa; (d) Ganymede	17
7	Camera Coverage and Resolution near Jupiter	18
8	Camera Coverage and Resolution near Europa	19
9	Percent Coverage at Jupiter	20
10	Photo Emitter Performance	23
11	Scanning Geometry	26
12	Camera Weight Data	30

List of Tables

1	SATELLITE ENCOUNTER ORBIT CHARACTERISTICS	3
2	SPIN SCAN TIMING CHART - JUPITER IMAGING	10
3	SPIN SCAN TIMING CHART - EUROPA IMAGING	10
4	SELECTED DATA FOR JUPITER AND THE GALILEAN SATELLITES	14
5	MAXIMUM PICTURE SEQUENCE	15
6	SPIN SCAN IMAGER CHARACTERISTICS	31
7	CAMERA GEOMETRY AND DATA CHARACTERISTICS AT JUPITER	32
8	CAMERA GEOMETRY AND DATA CHARACTERISTICS AT EUROPA	32

SPIN SCAN IMAGING AT JUPITER

Kenneth F. Sinclair*
Ames Research Center
Moffett Field, California 94035

Introduction

Television systems, operating as frame type imagers, have been used extensively in the planetary exploration program to date, but the use of spin scan imaging systems has been limited to Earth orbital applications. Because of the possible use of spinning spacecraft for early orbital outer planet missions, however, it is appropriate to consider the applicability of the spin scan imaging mode to these possible future missions.

Without some method of image motion compensation and/or great sensitivity (either through the use of large optics or one or more stages of image intensification), the performance of frame imagers used aboard a spinning platform is seriously limited by image smear. A spin scan camera, on the other hand, obviates most of these difficulties since the spinning motion of the platform is used to provide the scanning motion required to cover the imaged field. Thus, a spin scan camera and a spinning platform are complementary. However, experience to date with spin scan devices has come only from geostationary systems in Earth orbit. As a consequence, relative motion between the spacecraft and the surface being imaged has been small and the surface brightness has been adequate so that full frames could be acquired in a relatively short period of time even with a small telescope. At the outer planets, conditions will be far more severe. Relative spacecraft-surface motion can be great. Frame times will be long because of low light levels even with relatively large telescopes, and the spacecraft to planet range and phase angle may change considerably during the imaging period. In addition to these problems, the limited data transmission and storage capability of early outer planet

* Currently with XETEX, Inc., Belmont, California.

spacecraft will constrain the field of view, the spin rate, and the feasible number of detectors in the system.

The purpose of this study is to make a preliminary assessment of these problems and to determine the general feasibility of spin scan imaging from spinning platforms in outer planet orbiters. This study is limited to consideration of a typical orbiter mission to Jupiter with an orbit designed to provide repetitive close approaches to the Galilean satellites.

In the following section, the data requirements for imaging experiments at Jupiter and its satellites are reviewed. Next is a discussion of the spin scan camera and baseline camera selection. The third section covers operational considerations bearing on imager performance. Then, a physical camera model including relationships identifying the supporting requirements is developed and used to determine the characteristics of the baseline camera. The last section presents conclusions derived from the study and recommendations concerning further work.

Data Requirements for Imaging Experiments

One of the more interesting Jupiter orbiter mission options is one that not only includes the possibility of planetary observations, but also permits close multiple encounters with some of the major satellites.* Studies have shown that several feasible orbits exist which provide such multiple satellite encounters (refs. 1 and 2). In this paper, an orbit typical of the satellite encounter class of orbits has been selected for analysis. The characteristics of this orbit are shown in table 1 (ref. 2).

* Unfortunately, a stationary orbit at Jupiter ($2.25 R_J$, circular) requires a capture ΔV of 12.3 km/sec necessitating a large insertion stage well beyond the capability of current or projected launch vehicles. Too, the radiation hazard from a close-in circular orbit very likely precludes successful operation except for a very short period of time.

TABLE 1. SATELLITE ENCOUNTER ORBIT CHARACTERISTICS

Orbit Period, Day	14.222
Periapsis Radius, R_j	2.290
Apoapsis Radius, R_j	45.131

These orbits are interesting, of course, because they provide the opportunity to perform scientific experiments both at Jupiter and at some of its satellites. But this opportunity also poses some interesting problems for the imaging system. Imaging observations pertinent for Jupiter are primarily those related to the meteorology of the planet while those suitable for the satellites have a planetology orientation because of the thin or nonexistent atmospheres at these bodies. The resolution regimes for these two different classes of experiments are quite different. Since this study considers an early orbital mission to Jupiter, imaging experiments related to regional coverage are most appropriate (ref. 3). This experiment class emphasizes coverage rather than detailed resolution and should provide the bridge between Earth based measurements and follow-on more detailed measurements. Full disc measurements with resolution at least an order of magnitude better than that obtainable from Earth (about 300 kilometers) and more detailed images at a resolution of 10 kilometers with 100 percent coverage and a frame size of at least 10,000 kilometers would materially contribute to an understanding of regional meteorology at Jupiter (ref. 4). The specific observations that would be made include global cloud coverage, convective cells and turbulence, and cloud and cyclone formation. There are no stringent lighting constraints on the measurements but repetitive (every few minutes) images are desirable for cloud formation studies. Repeat coverage of the total area would be desirable a few times during an Earth year to observe the appearance and extent of relatively long term changes in the overall cloud cover and weather.

Imaging of the satellites of Jupiter would require much better resolution than that for the planet itself. Measurements with a resolution of about 1 kilometer with 100 percent coverage and a frame size consisting of at least a few hundred resolution elements would provide valuable data

on the planetology of these bodies. Observations of the structure of features, and surface topography and appearance could be made at this capability level. All of these measurements are most effectively made at low sun angles (20°) except for those boundaries between different rock types which are not delineated by surface relief. Such boundaries can be better observed with high sun elevation.

While the measurements outlined are a desirable goal for an early orbiter, it must be recognized that initial measurements providing synoptic coverage at considerably poorer resolution than that specified will, nonetheless, result in substantially improved knowledge about these bodies, provided that a significant improvement over Earth-based resolution is achieved.

Spin Scan Camera

Before assessing the feasibility of meeting the data requirements outlined above under expected operational conditions, a preliminary, or baseline, camera performance must be specified. Before that step, however, some description of the spin scan imaging approach is needed.

Camera Description. - In the spin scan camera, a point detector is positioned in the image plane of a telescope. This point detector measures the brightness of a very small region of the imaged scene contained within the total field of view. When the telescope is mounted on a properly oriented spinning platform the scene is systematically moved past this point detector, thus generating an analog signal corresponding to the brightness changes of a line across the scene. After each rotation of the platform, the telescope cone angle is moved (or, alternatively, a scan mirror is moved) through an angle subtended by the instantaneous field of view of the detector at the target. With the combination of the spin and step motions, a raster covering the area to be imaged is gradually developed. This raster is essentially analogous to the raster scan used in reading out the stored image on a television tube target after exposure. The difference is that in the television case the raster reads out a static scene in non-real time whereas the spin

scan raster is reading out the scene in real time. The geometry for a typical imaging sequence is shown in figure 1.

Instead of a single detector in the image plane as discussed above, a spin scanner can have several detectors mounted so that their instantaneous fields are contiguous or overlapping, thus permitting coverage of a larger region on the surface for each rotation of the platform. Detectors sensitive in different spectral regions or appropriately filtered can also be used to provide multi-band spectral data. When several detectors are used, an equal number of analog signal streams are generated and the data rate is correspondingly increased. Figure 2 illustrates the way such a multiple data stream is digitized and converted to a single sequential data stream. The performance of the various configurations outlined depends on the components employed and the operational conditions under which the spin scanner is used.

Camera Selection. - Figure 3 shows camera performance as a function of instantaneous field of view (IFOV) for several different target ranges normalized to the planetary radius of Jupiter. Based on this information, and the data requirements outlined earlier, an IFOV of 100 microradians was selected as a baseline. This capability would permit a pixel resolution equivalent to about 10 km at periapsis and, based on prior experience, appears to be attainable.

Actual camera selection depends on a number of other factors including the data handling and telemetry rate constraints of the spacecraft system, the useful operating spin-rate range, and of course, the state-of-the-art for camera components. For this study, a relatively modest spacecraft system of the Pioneer type was assumed (ref. 5). No data storage, except short term buffering, was desired, and a telemetry rate of ten kilobits per second was assumed. The spin-rate range for an RTG-powered spacecraft was assumed to be 2-10 rpm. Using the constraints shown, cameras at several different performance levels were compared.

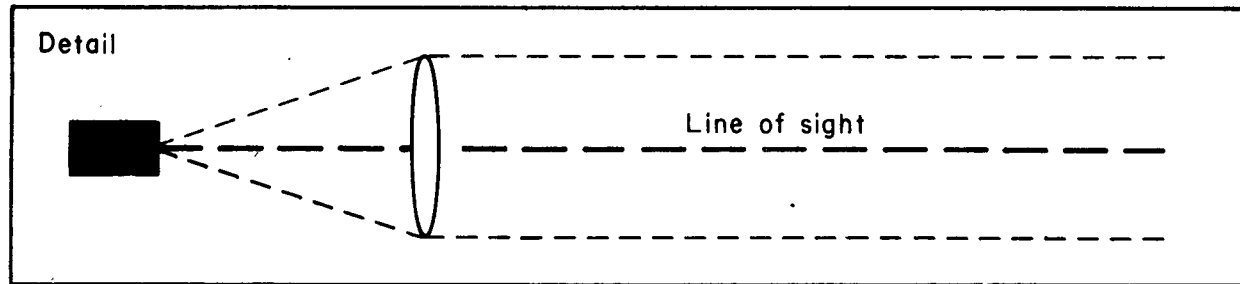
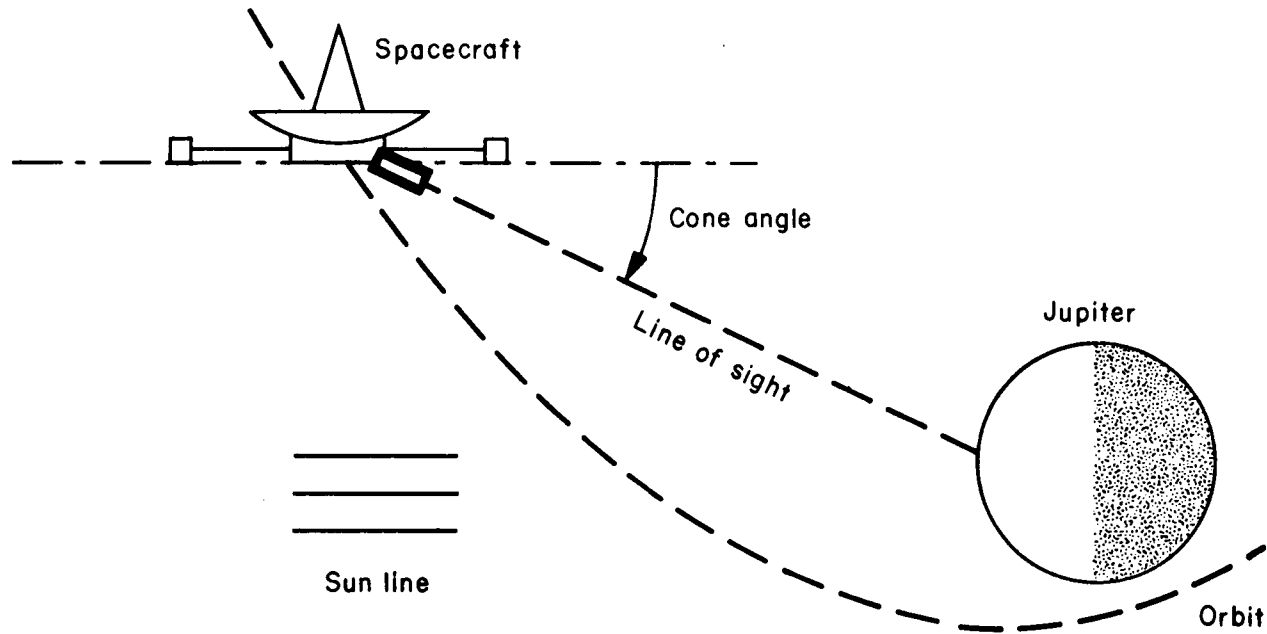


Figure 1. - Typical Spacecraft and Camera Geometry near Jupiter.

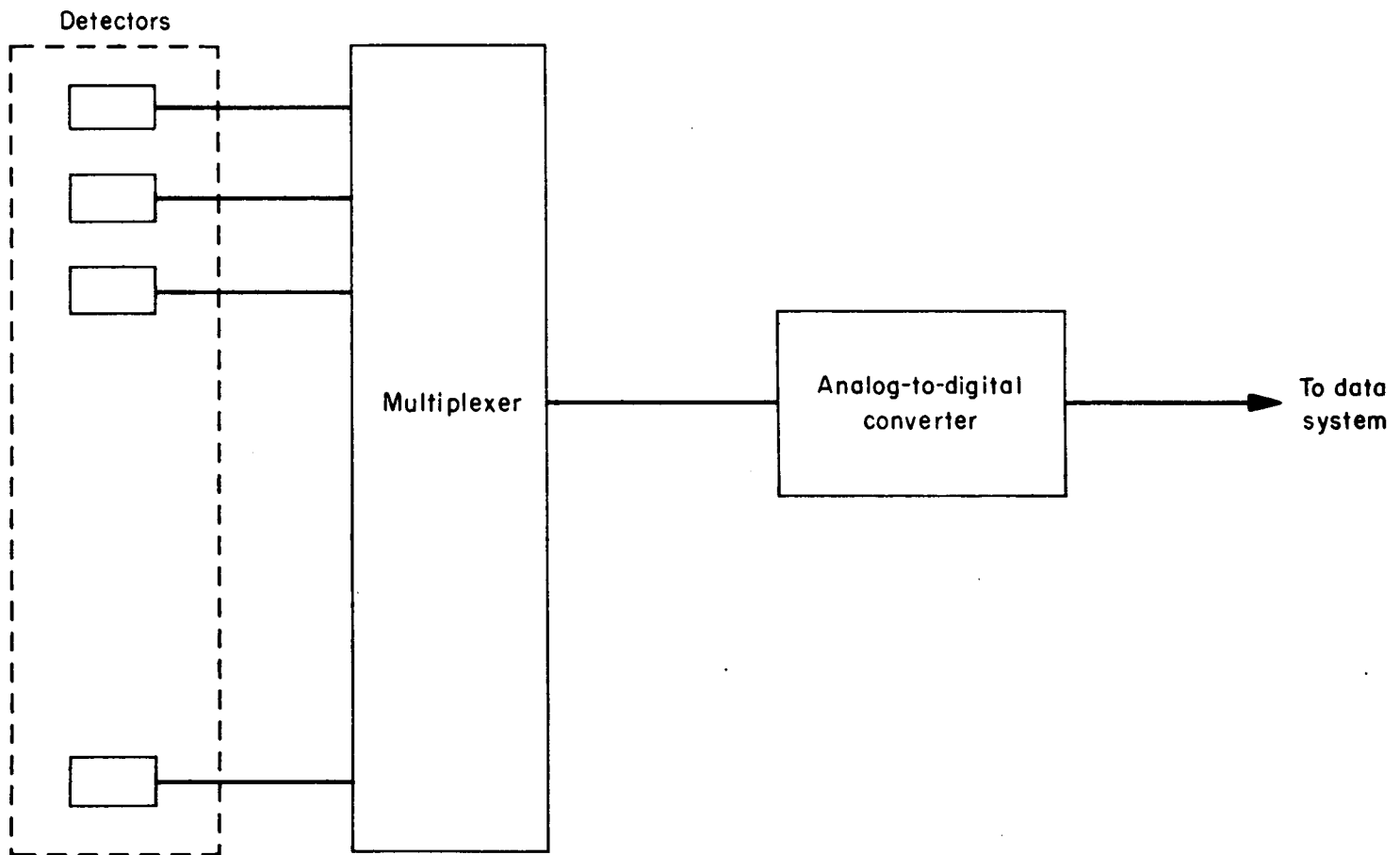


Figure 2. - Multi-Detector Data Handling.

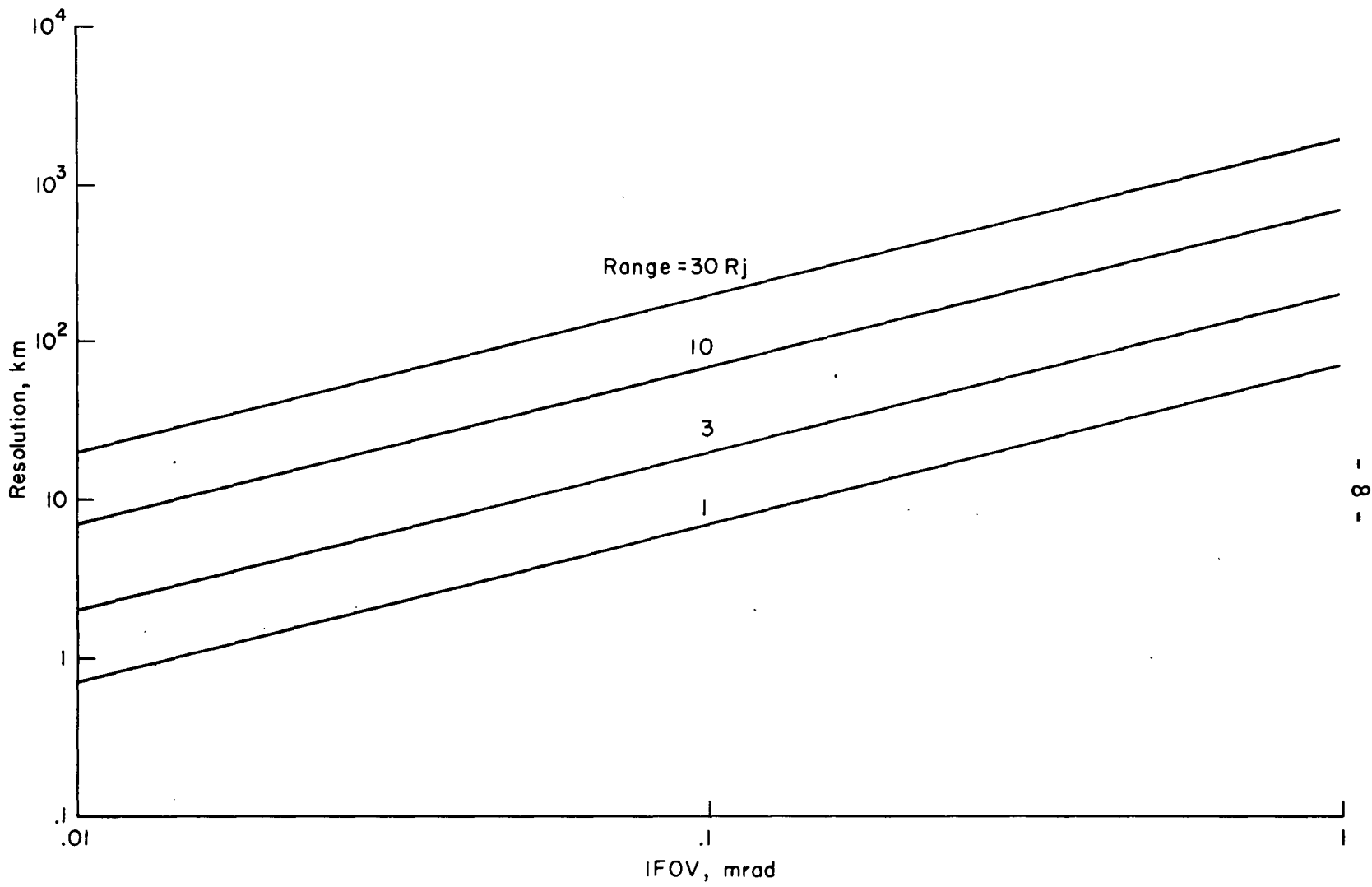


Figure 3. - Camera Resolution.

The performance of such systems with a single detector at Jupiter and Europa is shown in tables 2 and 3 respectively. A single detector system of this type approaches the resolution requirements defined earlier with a very modest telemetry requirement for the range of spin rates considered. The telemetry rates shown are based on the use of buffer storage and continuous transmission during the entire spin cycle.

Because of the low telemetry rates shown in the tables, multiple detector configurations can be used to decrease the frame time with a corresponding increase in the telemetry rate. This is especially important in view of the long frame times shown in the tables. Because of the short Jupiter day (~10 hours), long frame times pose severe picture reconstruction problems. To minimize this problem, planetary rotation during exposure of the frame should be held to a small fraction of a revolution. An arbitrary goal of 0.1 revolutions, or about 60 minutes frame time, has been used as the upper limit here. At frame times of this duration, scan line distortion is not large and the fractional coverage loss is small. In some cases, especially near periapsis or during satellite flybys, the change in phase angle during exposure may be dominant and frame times significantly shorter than sixty minutes may be desirable. Based on these considerations, a ten detector system operating at a spin rate of 5 rpm appears to meet most of the requirements outlined. The data, resolution, and frame time characteristics of such a system are shown in figure 4. The performance of this camera under operational conditions will be assessed next.

Operational Considerations

The orientation of the example elliptical orbit is shown in figure 5. Because of perturbation effects caused by the satellites, some ΔV is required periodically to trim the orbit. These perturbations and the normal motions of the satellites cause variations in the satellite encounter geometry from orbit to orbit. This diagram is for the second orbit of the example mission involving three-satellite

TABLE 2. SPIN SCAN TIMING CHART - JUPITER IMAGING

Dist. R _j	Angular Res. μr	Spatial Res. (km)	Spin Rate (rpm)	Lines Per Frame	Pixels Per Line	Bits Per Line	Data Xmit Period (sec)	Telem Rate (bps)	Total Frame Time Δt (min)
20	100	142.6	2	1000	1000	6 k	30	.2 k	500
			5	1000	1000	6 k	12	.5 k	200
			10	1000	1000	6 k	6	.10k	100
10	100	71.3	2	2000	2000	12 k	30	.4 k	1000
			5	2000	2000	12 k	12	1. k	400
			10	2000	2000	12 k	6	2. k	200
3*	100	14.3	2	400	4375	26.2k	30	.87k	200
			5	1000	1750	10.5k	12	.87k	200
			10	2000	866	5.2k	6	.87k	200

* Full disc coverage not possible.

TABLE 3. SPIN SCAN TIMING CHART - EUROPA IMAGING

Dist. R _j	Angular Res. μr	Spatial Res. km	Spin Rate (rpm)	Lines Per Frame	Pixels Per Scan	Bits Per Line	Data Xmit Period (sec)	Telem Rate (bps)	Total Frame Time Δt (min)
1.82	100	12.7	5	240	240	1.44k	12	.12k	50
0.56	100	4.0	5	580	775	4.65k	12	.39k	120
0.28*	100	2.0	5	250	1550	9.3 k	12	.78k	50

* Full disc coverage not possible.

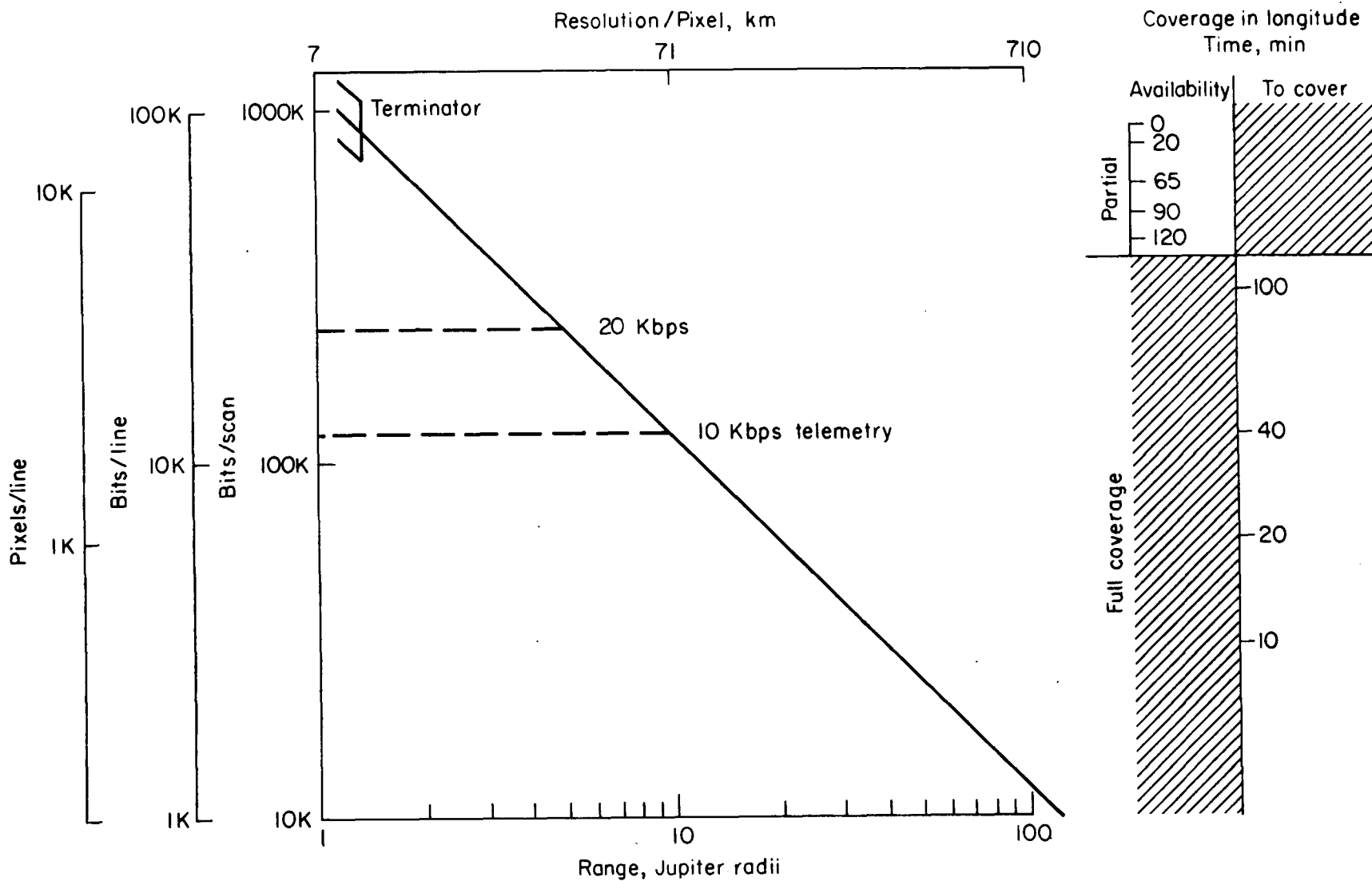


Figure 4. - Camera Performance Characteristics

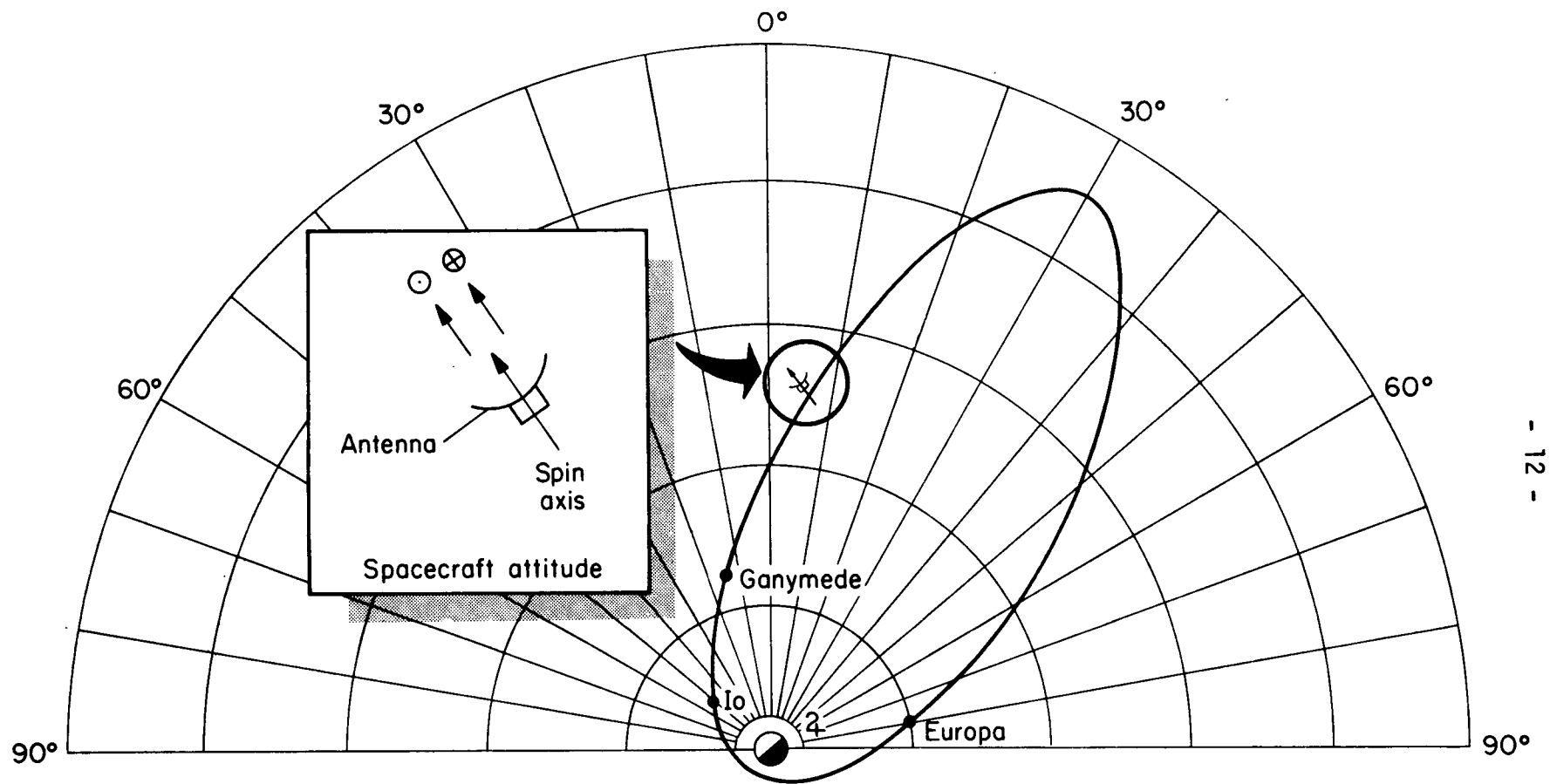


Figure 5. - Typical Jupiter Orbit.

(Ganymede, Io, and Europa) encounters at relatively close range. Certain characteristics of these satellites and Jupiter are given in table 4.

To simplify spacecraft communications antenna pointing problems, it is assumed that the spacecraft spin axis will be pointed towards Earth during the entire mission with the antenna rigidly mounted to the spacecraft with its look axis colinear with the spin axis (see figure 5). The camera cone angle required is then determined by the Earth-spacecraft-target angle which, of course, varies depending on the orbital position of the vehicle. The cone angle is changed after each revolution of the vehicle to provide contiguous coverage (with some overlap) across the frame. The ratcheting step size required depends on the number of detectors, the IFOV, and the relative spacecraft-target motion. At large distances from Jupiter, the number of detectors and IFOV are the dominant considerations. Near Jupiter periapsis and for the satellite encounters, the relative motion must also be considered.

An image sequence plan for orbit two is shown in table 5. This plan assumes that the maximum possible number of images, consistent with the science objectives, will be obtained. Based on this assumption, 704 frames of Jupiter, 7 of Ganymede, 6 of Io and 6 of Europa can be obtained on this orbit. During each sequence, the target-spacecraft range and, hence, the resolution and image acquisition time change. These variations have been accounted for in constructing the sequence plan. There is also a variation in phase angle (sun-target-spacecraft angle) during each frame and from frame to frame. The phase angle variation with range is shown in figure 6 for Jupiter, Ganymede, Io, and Europa. (From ref. 2). For distant images there is a minimal change in range during frame acquisition. Close to the target, however, the variation in range and therefore the variation in phase during this time is significant, and as a result, image reconstruction is made more difficult.

The resolution/coverage performance of the baseline system at Jupiter and Europa at various ranges is depicted in figures 7 and 8, respectively. Coverage at Jupiter as a function of resolution is shown in figure 9. The limiting surface resolution is about 9 km because the spacecraft

TABLE 4. SELECTED DATA FOR JUPITER AND THE GALILEAN SATELLITES
 (Incident Energy 433 foot candles)

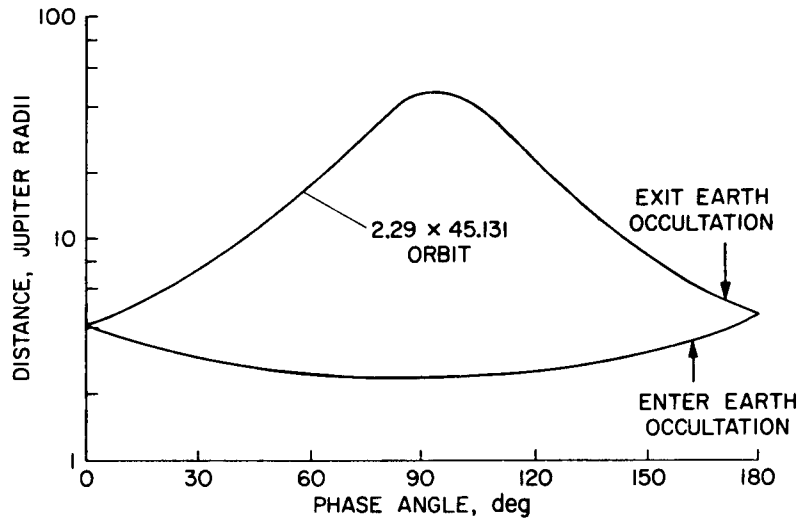
	<u>Albedo</u> *	<u>Luminance</u> (ft lamberts)	<u>Radius (km)</u>	<u>Orbit</u> <u>R_j</u>
Jupiter	0.41	178	71,372	---
Io	0.92	398	1,670	5.9
Europa	0.85	368	1,460	9.4
Ganymede	0.49	212	2,550	15
Callisto	0.26	113	2,360	25.4

* Spectral band - 0.4-0.7 μm

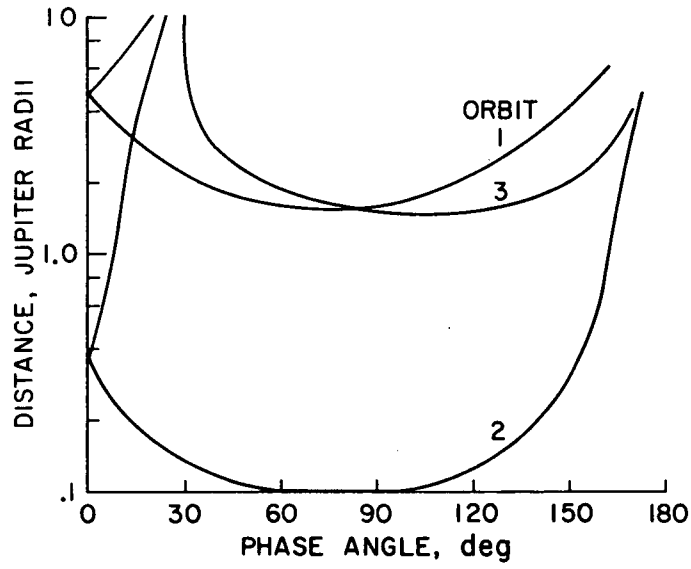
TABLE 5. MAXIMUM PICTURE SEQUENCE

<u>True Anomaly (Deg)</u>	<u>Picture Sequence Start*</u>	<u>Finish</u>	<u>Max. Frames Full/Partial</u>	<u>Target</u>	<u>Phase Angle (Deg)</u>	<u>Range R_j</u>
121	0.3099				5.6	1.338
			6/0	Europa		
127		0.3867			90	0.262
180	7.1142				90	45.131
			680/0	Jupiter		
215+		13.3974			70	16.197
216	13.3988				33.6	1.332
			6/1	Ganymede		
218		13.4792			48	0.135
218+	13.4806				55	15.130
			19/0	Jupiter		
243+		13.9654			28	7.390
244	13.9668				23.5	1.313
			5/1	Io		
253		14.0300			90	0.244
253+	14.0314				20	5.923
			0/5	Jupiter		
360		14.2284			90	2.29

* Days from injection

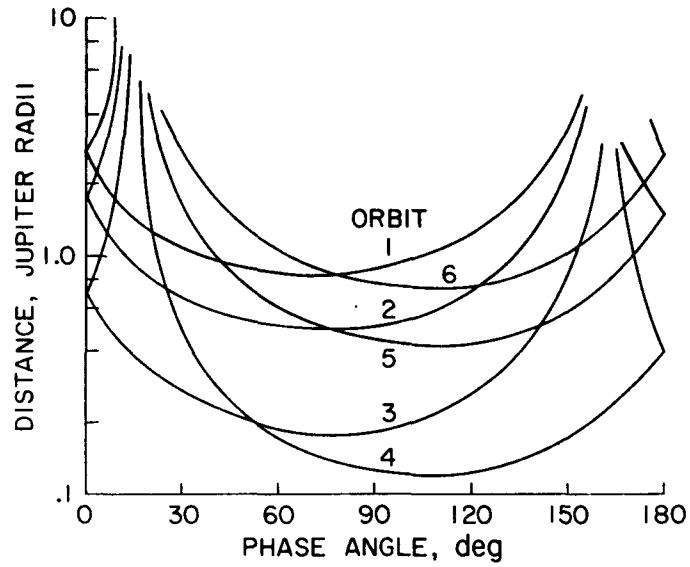


(a) Jupiter

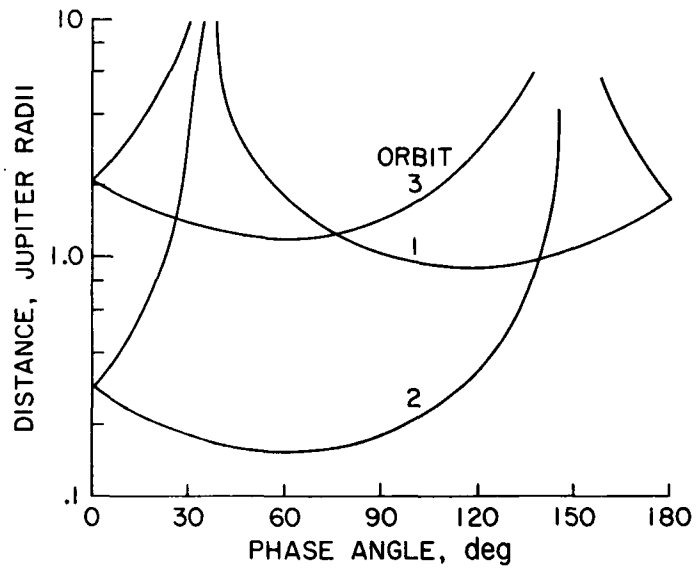


(b) Io

Figure 6. - 1976 Encounter Characteristics.



(c) Europa



(d) Ganymede

Figure 6. - Concluded.

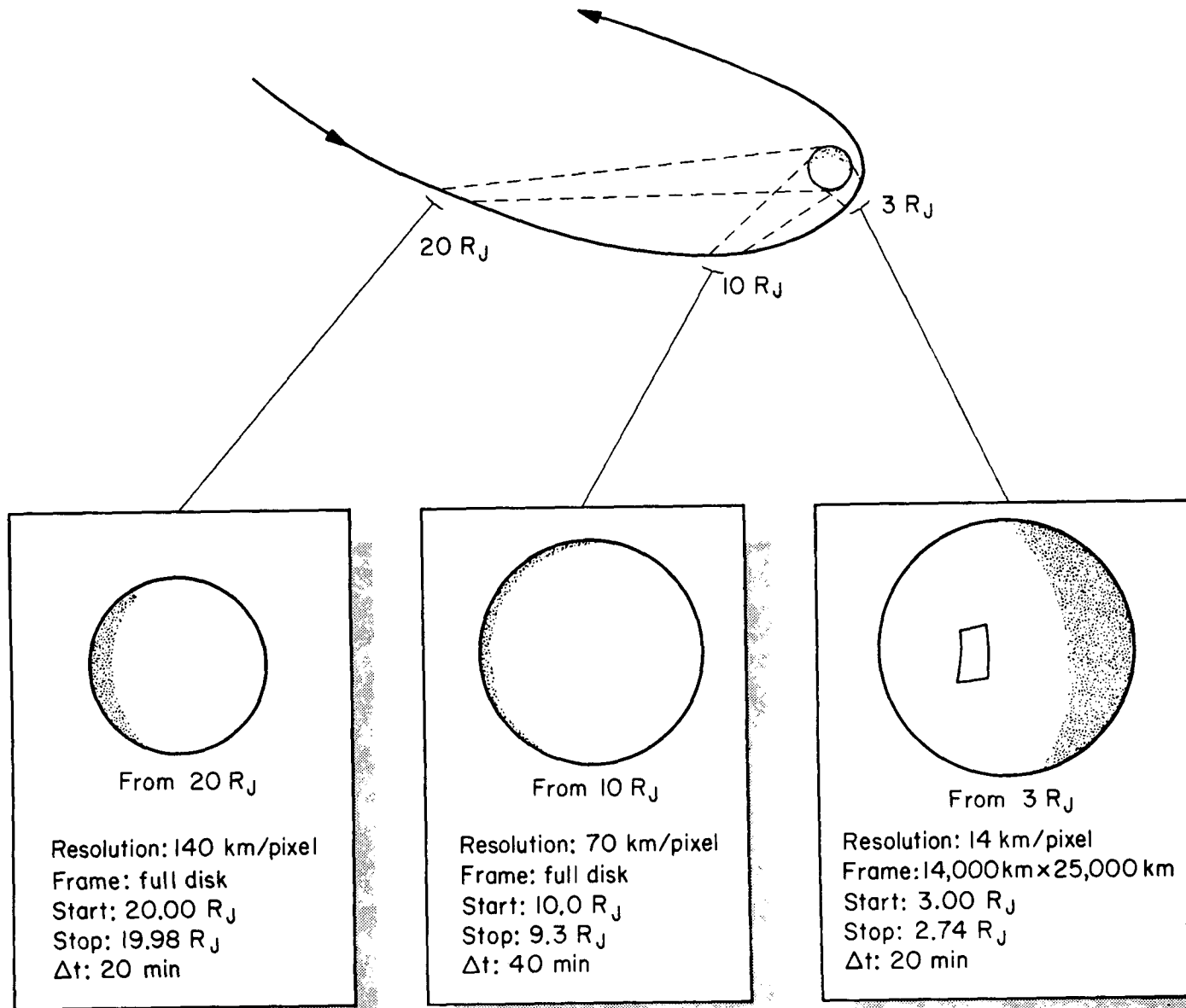


Figure 7. - Camera Coverage and Resolution near Jupiter.

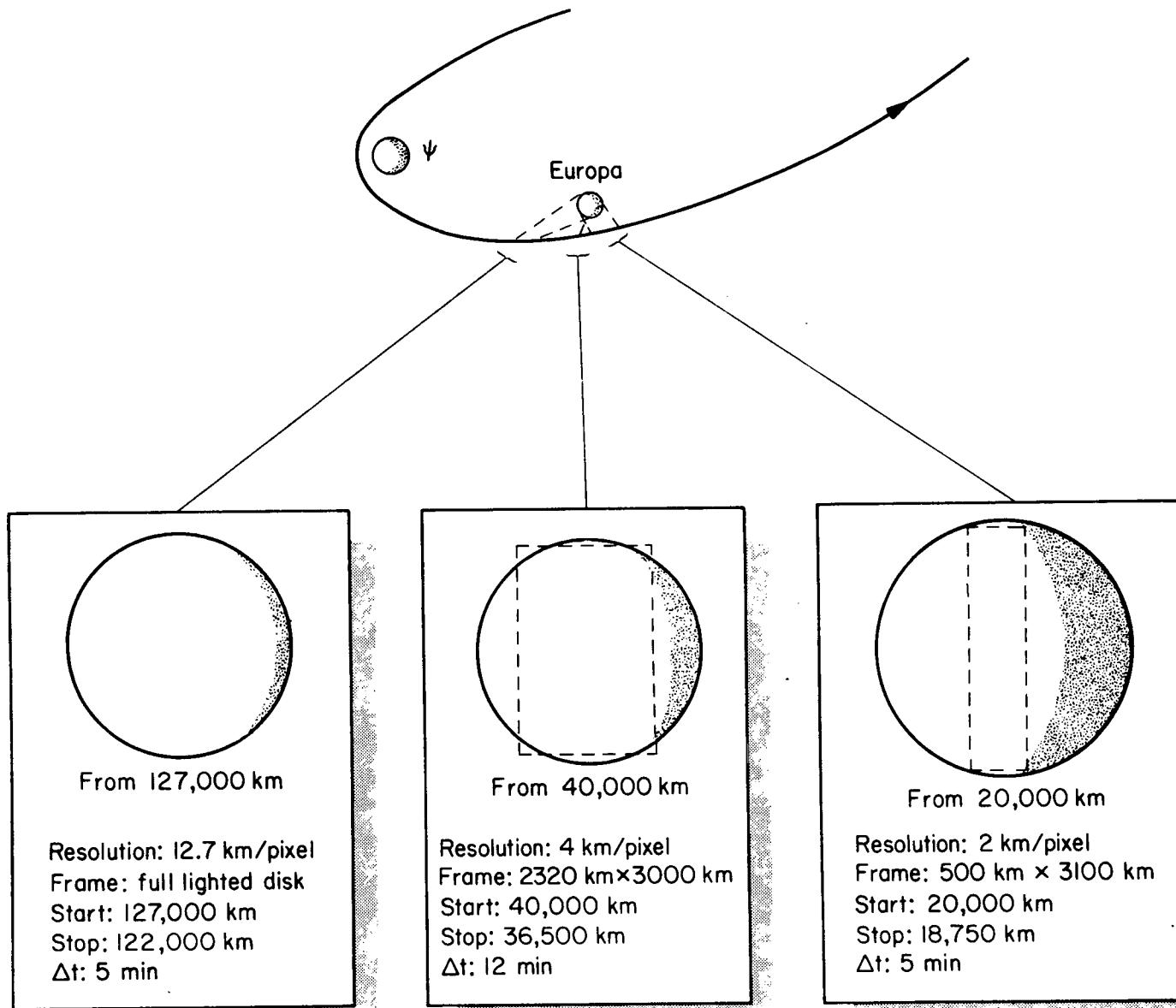


Figure 8. - Camera Coverage and Resolution near Europa.

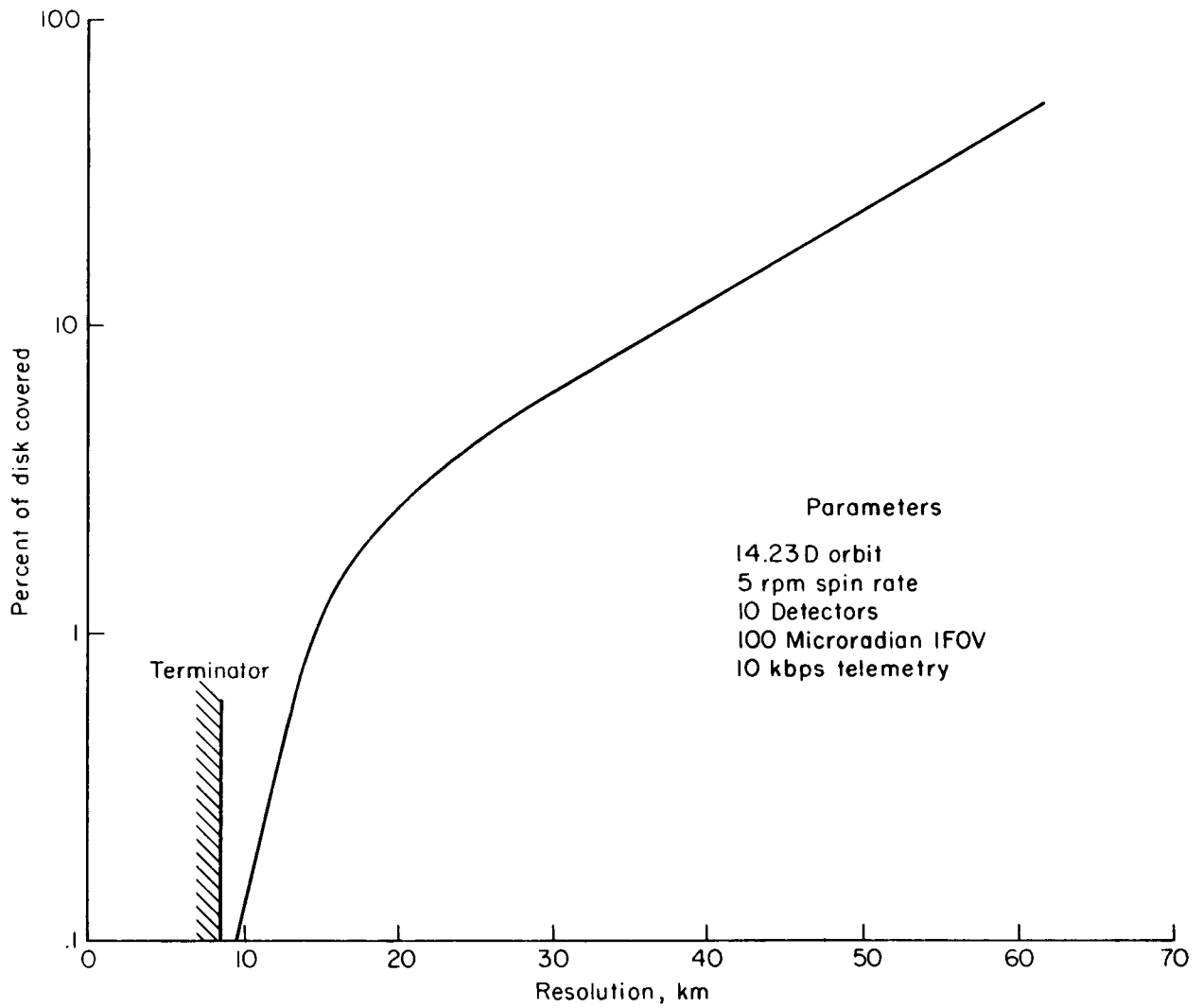


Figure 9. - Percent Coverage at Jupiter.

nadir crosses the terminator and thus enters the dark side of the planet at the range where this resolution is just possible.

Preliminary Camera Design

The size, weight, and complexity of a camera exhibiting the performance of the baseline system depends on a number of factors such as available light, detector characteristics, etc. In this section of the report, a spin scan camera model will be developed and then used to determine the gross design of the baseline system. The model includes the physical laws governing performance, the state-of-the-art characteristics for the components, scaling relationships identifying the support requirements, e.g., power, weight, data rate, etc., and the effects of scan geometry on average data rate.

The design of the baseline camera, based on this model, represents a first order estimate of the system characteristics and is useful primarily to establish the general feasibility of the approach.

Camera Model

Optical System: Because of the relatively large light collection capability required for outer planet missions, relatively large optics are required. Consequently, to minimize system weight, catoptric systems are normally used. Because of the very small instantaneous field of view that characterizes spin scan imagers, reflecting optics of excellent performance are feasible. While many different configurations are possible, a Cassegranian telescope will be considered here. The light collection capability for such a system is given by:

$$I = AB^2t$$

where A is the effective area of the collecting optics
B is the instantaneous angular field of view, and
t is the optics and filter transmission factor.

The effective area is:

$$A = A_p - A_s$$

where A_p is the area of the primary, and
 A_s is the area of the secondary.

Substituting for the primary and secondary areas, we have:

$$A = \frac{\pi}{4} \left[D^2 - \left(\frac{0.5 D}{N} \right)^2 \right] \quad (1)$$

where D is the diameter of the primary, and
 N is the focal ratio of the system.

Since the focal ratio is given by:

$$N = \frac{F}{D_e}$$

where

$$D_e = \sqrt{\frac{4A}{\pi}}$$

Equation 1 can be rewritten as:

$$A = \frac{\pi D^2 F^2}{4F^2 + D^2}$$

And, thus, the intensity of the collected radiation is equal to:

$$I = \frac{\pi D^2 F^2}{4F^2 + D^2} B^2 t$$

Detectors: Over the visual band photomultiplier detectors generally have a significant advantage over other types because of their relatively high quantum efficiency and high internal gain. Figure 10 shows the performance of currently used photo emitters over the spectral range of interest (ref. 6). It is convenient to express the performance of photo

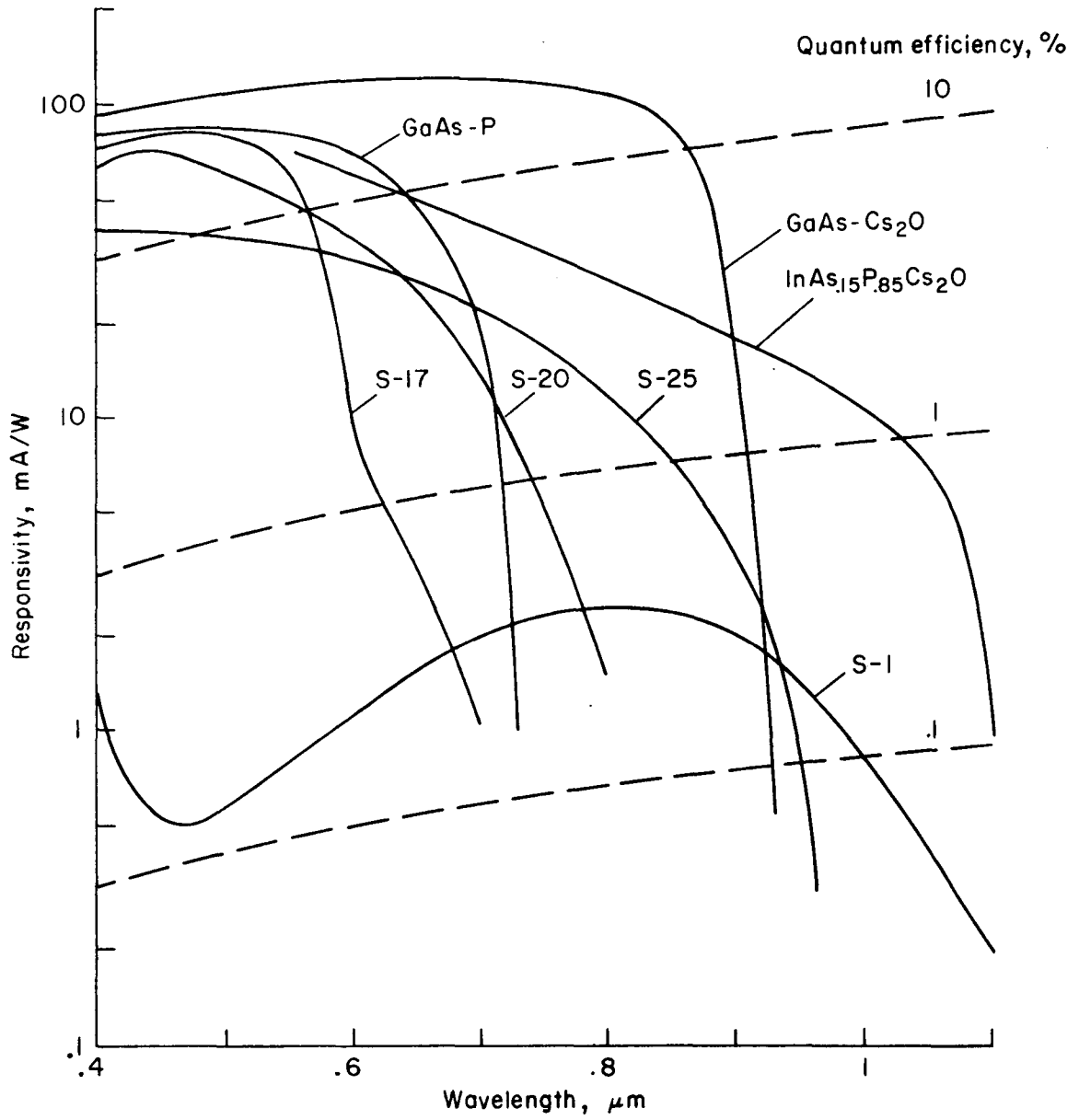


Figure 10. - Photo Emitter Performance.

emitters in terms of responsivity in milli-amperes per watt. The power incident on the photo surface when coupled to an optical system of the type described above, then is:

$$P = N_{\lambda} \Delta\lambda AB^2 t$$

Where N_{λ} is the spectral radiance, and
 $\Delta\lambda$ is the wavelength interval

And the current produced by a photo emitter is given by:

$$i = RPM$$

where R is the cathode responsivity (current per unit energy), and
M is the current multiplication factor

Because of the large gain with photomultiplier systems, the noise is primarily a function of two factors: the shot noise associated with the signal itself; and that introduced due to the statistics involved in the secondary emission process which amplifies both signal and primary shot noise currents (ref. 6). Thus, the mean square shot noise of the output current at the anode of the photomultiplier is:

$$i_n^2 = 2q (i + i_d) M^2 F f$$

where q is the charge on the electron
 i_d is the dark current
f is the bandwidth, and
F is the noise factor.

The noise factor is given by:

$$F \approx \frac{\Delta}{\Delta - 1} \quad \Delta \gg 1$$

where Δ is the average gain per stage of the photo tube.

For a typical stage gain, Δ , of 3, the noise factor, F , is about 1.5. This value will be used in subsequent computations.

The overall signal-to-noise ratio for the photomultiplier tube, then, can be written:

$$S_n = \frac{i}{i_n} = \frac{\text{PRM}}{[3q (\text{PR})M^2f]^{1/2}} = \left[\frac{\text{PR}}{3qf} \right]^{1/2}$$

Performance of a Buffered System: If it is assumed that the energy collected by the optical system described above is delivered to the photo-cathode of the photomultiplier tube without loss, the total system performance in terms of signal-to-noise ratio is defined by:

$$S_n = \left[\frac{\frac{D^2 F^2}{4F^2 + D^2} B^2 t N_\lambda \Delta \lambda R}{3qf} \right]^{1/2}$$

Data Rate: The data rate is determined by the number of pixels per scan, the number of simultaneous scans, the gray scale per pixel, and the acquisition time. Thus, the data rate is given by:

$$D_r = \frac{2S n G}{B r t_a} \quad (2)$$

where S is half the active scan arc length
 n is the number of simultaneous detectors used
 G is the grey scale
 B is the instantaneous field of view
 r is the range to the target, and
 t_a is the data acquisition time.

The factor t_a , is determined by camera geometry and spin rate. The generalized geometry for a spin-scan camera is shown in figure 11. As shown by the figure, the data acquisition time, t_a , is a variable depending on the spacecraft target range, the size of the target, the cone angle of the scan, and the spin rate of the spacecraft.

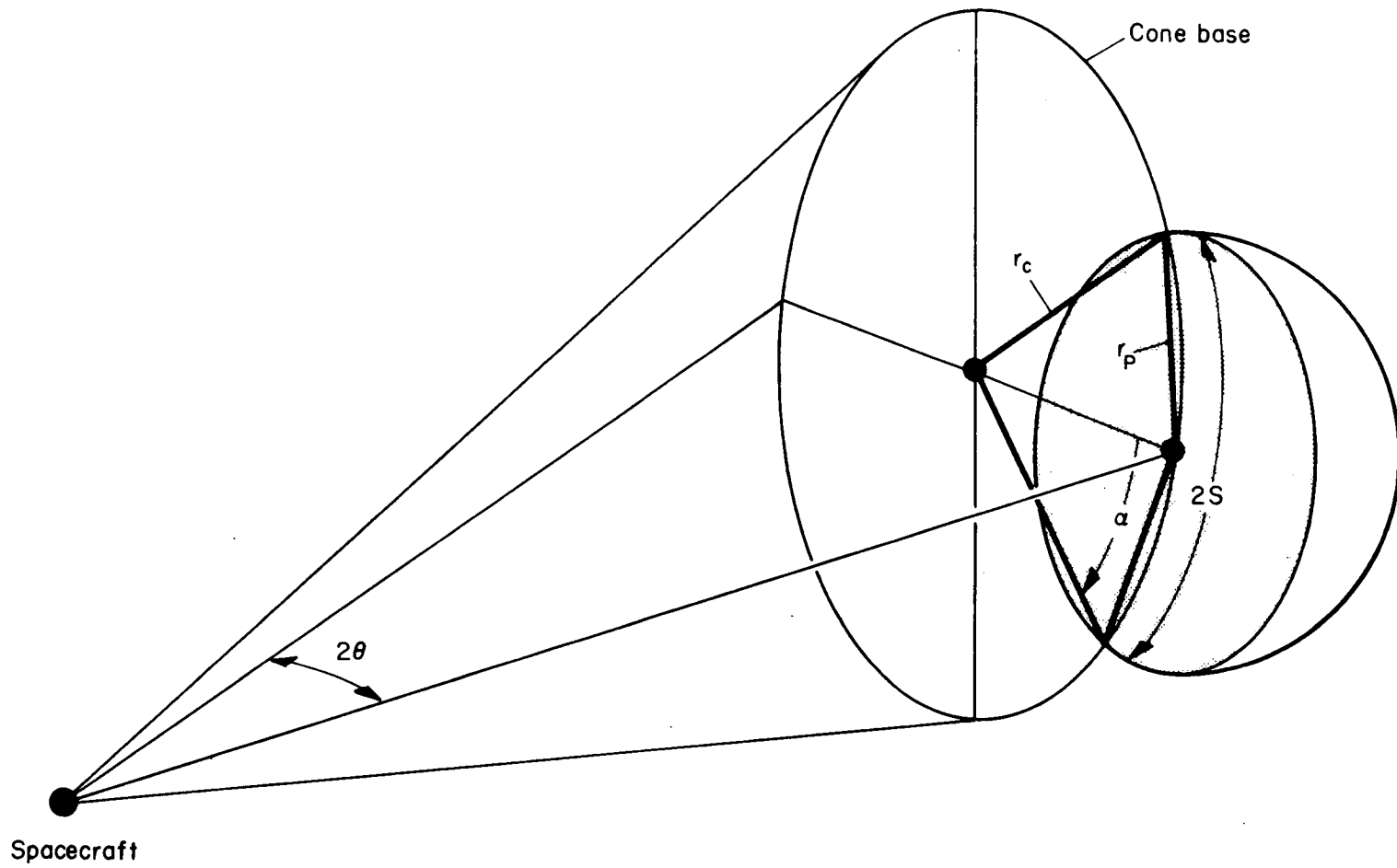


Figure 11. - Scanning Geometry.

The fraction of time out of each spin cycle during which data is acquired is given by:

$$t_a = t \frac{2\alpha}{2\pi} = t \frac{\alpha}{\pi}$$

where t is the time per revolution of the spacecraft

α is the half angle subtended at the base of the cone by the scan arc, in radians.

Since the time per cycle is:

$$t = 60/\omega$$

where ω is the vehicle spin rate in rpm, the acquisition time can be rewritten:

$$t_a = 60 \alpha / \omega \pi$$

where t_a is in seconds.

The angle subtended by half the scan arc is:

$$\alpha = S/r_c$$

where r_c is the radius of the cone base (see Figure 11).

The worst case condition is given by the longest scan arc for any given target since this represents the greatest data load for a single scan. This arc is defined by the scan circle that passes through the poles of the planet and half of this arc is given by:

$$S = r_c \sin^{-1} \frac{r_p}{r_c} \text{ (through poles)}$$

For the worst case condition then, the acquisition time is:

$$t_a = \frac{60 \sin^{-1} r_p / r_c}{\omega \pi}$$

Since the cone radius is:

$$r_c = r \sin \theta,$$

where r = range to planet

θ = cone half angle,

the expression for data acquisition time can be written:

$$t_a = \frac{60 \sin^{-1}(r_p/r \sin \theta)}{\omega \pi}$$

Substituting in equation (2) for S and t_a , we have:

$$D_r = \frac{r \sin \theta (\sin^{-1} r_p/r \sin \theta) n G \omega \pi}{60 B r (\sin^{-1} r_p/r \sin \theta)}$$

Thus, the data rate can be written:

$$D_r = \frac{r \sin \theta n G \omega \pi}{60 B}$$

The total data load for the worst case scan (that is, through the poles) is given by:

$$D_t = \frac{\sin \theta (\sin^{-1} r_p/r \sin \theta) n G}{B}$$

The data rate averaged over the entire spin cycle, which is representative of the required transmitted data rate assuming that buffer storage adequate for one collection period is provided, is given by:

$$D_a = \frac{2S n G}{B r t} = \frac{S n G \omega}{30 B/r}$$

Size, Weight, and Power: The size and weight of a spin scan camera of moderate to high resolution is generally dominated by the telescope. Figure 12 shows total weight versus primary aperture size for the spin scan systems that have been flown or are now in development. The smallest instrument shown on the curve, the Pioneer 10 and 11 imaging photopolarimeter, is probably anomalously heavy because of the varied functions it must perform. As a consequence, considerable electronic and optical complexity is required. The largest system shown on the curve, the visible infrared spin scan radiometer (VISSR), is representative of the present state-of-the art in that an all-beryllium structure and all-beryllium optics are employed.

Baseline Camera. - A preliminary estimate of the baseline camera characteristics based on the relationships developed above is given in table 6. This estimate is based on target luminance of 200 foot Lamberts with a phase angle of 60° and a contrast at the camera of 1.3:1. These values are assumed to approximate "worst case" conditions for Jupiter and the Galilean satellites.

The required camera cone angles (angle relative to spacecraft spin axis) for typical encounters at Jupiter and Europa and the consequent data acquisition characteristics are given in tables 7 and 8. For these conditions, onboard buffer storage with a maximum capacity of 120 kilobits is required with a read-in rate capability of 267 kilobits per second.

Concluding Remarks

The rather modest camera outlined, i.e., 12 kg and 20 watts, should provide extremely useful images of Jupiter and its near satellites. On the type of orbit discussed here, the complementary combination of the spin scan imaging technique and the spinning spacecraft is obvious, but it is useful to review some of the specific benefits and the problems of this combination. Such a camera imposes very limited support requirements on the spinning spacecraft because the relatively long frame times effectively size the data stream to suit the storage and telemetry constraints of the

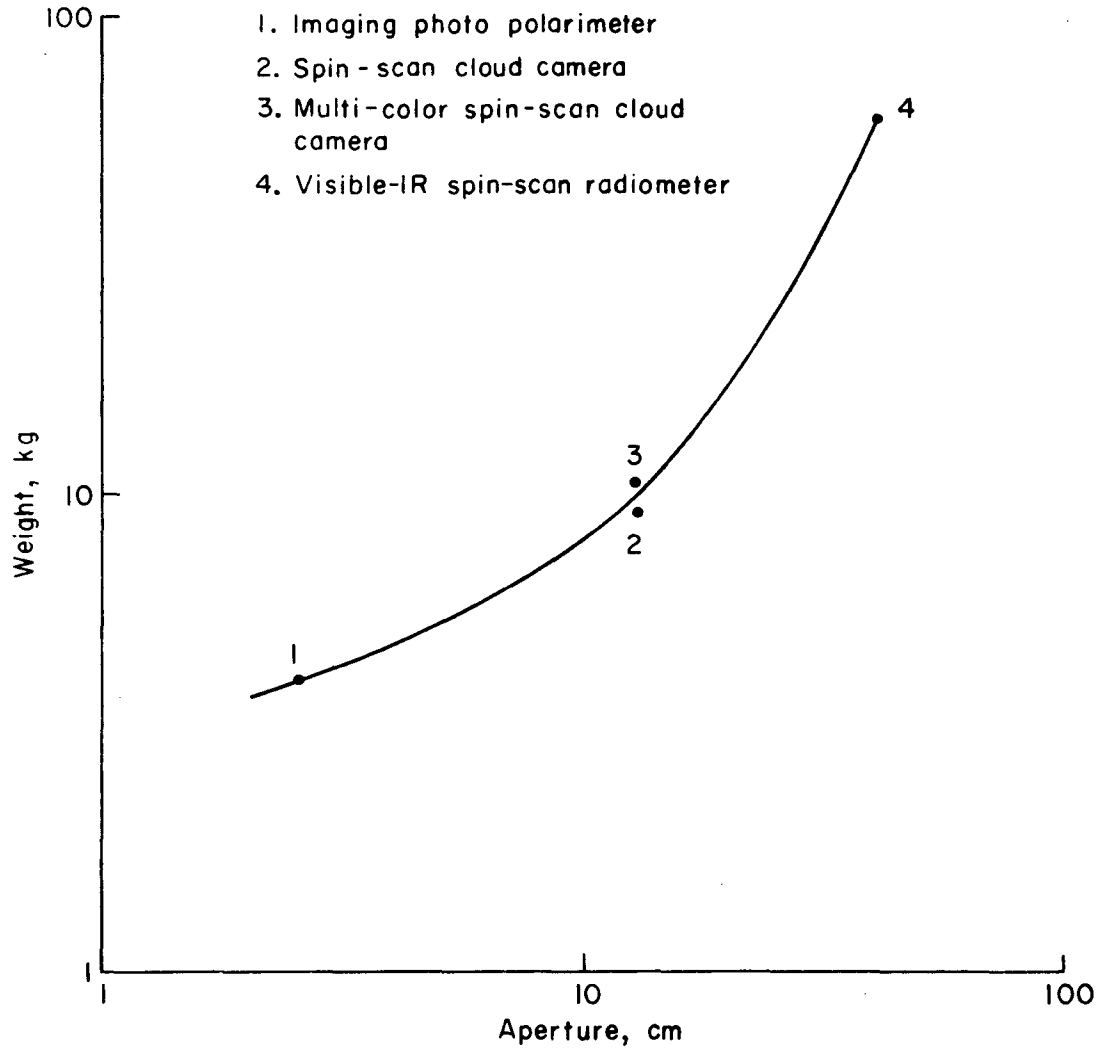


Figure 12. - Camera Weight Data.

TABLE 6. SPIN SCAN IMAGER CHARACTERISTICS

- MULTI-DETECTOR SPIN SCAN CAMERA
- SPECTRAL BAND 0.4-0.7 μ (OTHERS OPTIONAL)
- 10 DETECTORS (PMT'S OR CCM'S)
- IFOV = 100 μ RAD EACH DETECTOR
- 6" DIA f/4 REFLECTIVE OPTICS
- VARIABLE CONE HALF ANGLE: 5° - 175°
- WEIGHT AND POWER: 12 KG, 20 W
- SPIN RATE: 5 RPM

TABLE 7. CAMERA GEOMETRY AND DATA CHARACTERISTICS AT JUPITER

Dist. R_j	Cone Half Angle	Angle Subtended by Scan	Bits Per Scan	Data Acquis. Period (sec)	Bit Rate to DSU (kbps)	Telem. Rate (kbps)	Frame Time (min) (2)
20	29°	13°	60k	0.4	150 k	5	20
10	7°	110°	120k	3.7	32.8k	10	40
3 (1)	58°	11.8°	105k	.39	267 k	8.7	20

(1) Frame height 25,000 km, S = 12,500 not full.

(2) Time for complete image

TABLE 8. CAMERA GEOMETRY AND DATA CHARACTERISTICS AT EUROPA

Dist. R_j	Cone Half Angle	Subtended Angle	Bits Per Scan	Data Acquis. Period (sec)	Bit Rate to DSU (kbps)	Telem. Rate (kbps)	Frame Time (min)
1.82	2.8°	24.8°	14.4	.82	17.6	1.2	5
0.56	30°	8.4° ^b	46.5k	0.28	166	3.9	12
0.28	8°	60°	93.0k	2.0	47	7.8	55

vehicle. These considerations are vital to the relatively simple spinning spacecraft contemplated for some future outer planet missions.

While long frame times are advantageous from a data handling standpoint, they do complicate the ground reconstruction problem because of relative spacecraft-target motion during frame generation and the change in phase angle during the frame. In addition, the relatively small number of frames possible per pass, particularly at the satellites, is a disadvantage.

Future work should address the effects of these disadvantages on the usability of the imagery and should detail the nature of the ground reconstruction equipment and software required to produce a satisfactory rectified copy at output rates consistent with the production capabilities of an orbiter. The ancillary data regarding position, nutation rates, etc., required from the spacecraft to permit reconstruction must also be completely specified.

The serious problems posed by the Jupiter radiation belts on such an orbiting mission have not been discussed in this paper, but every effort must be made to harden the camera and spacecraft components sufficiently so that reasonable life can be expected in these radiation zones. Both transient and permanent radiation effects must be considered since the electro-optical devices used in spin scan cameras, such as photomultiplier tubes and channeltrons, are especially sensitive to both transient and permanent radiation effects. In addition, the materials used in some types of fiber optics and tube envelopes are sensitive to radiation. The light transmission characteristics of these components can be seriously degraded with radiation dose and, in addition, certain materials will luminesce during radiation bombardment creating spurious output signals or damaging sensitive components. Radiation hardening techniques must be used on the semi-conductor components and the storage devices also to insure reliability and long life. All of the system components should be examined in the light of postulated Jupiter radiation belt models and suitable steps taken to insure survival.

References

1. Niehoff, John C., "Touring the Galilean Satellites," AIAA 70-1070, 1970.
2. Swenson, Byron L.; Tindle, Edward L.; and Manning, Larry A., "Preliminary Mission Designs for Jupiter Orbiter Missions," NASA TM X-2565, May 1972.
3. Sinclair, K. F., "Communications Implications of Future Unmanned Planetary Missions," International Colloquium on Space and Communications, Paris, France, April 1971.
4. Klopp, D. A., et al, "Orbital Imagery for Planetary Exploration, Volume II, Definitions of Science Objectives," NASA CR-73451, 1969.
5. "Study of Follow-on Pioneer Missions to Jupiter," TRW Systems Group, August 1971, NASA Contract NAS2-6454.
6. Melchior, H.; Fisher, M. B.; and Arams, F. R.; "Photodetectors for Optical Communications Systems," Proceedings of the IEEE, October 1970.